metals

MDPI

Article

Effect of Heat Treatment on the Microstructure and Mechanical Properties of a Ti-TiAl Laminate Composite

Wei Sun [1,*], Ning Cui [1], Yongjun Su [2], Shuling Zhang [1], Tiewei Xu [1], Xiaopeng Wang [3] and Fantao Kong [3]

[1] School of Mechanical and Automotive Engineering, Qingdao University of Technology, Qingdao 266520, China
[2] Department of Mechanics, College of Engineering, Lishui University, Lishui 323000, China
[3] State Key Laboratory of Advanced Welding and Joining, Harbin Institute of Technology, Harbin 150001, China
* Correspondence: sw290214281@163.com

Abstract: The effect of an innovative two-step heat-treatment process on the microstructure and mechanical properties of a Ti-TiAl laminate composite fabricated by hot-pack rolling was studied in this paper. After heat treatment, the fracture toughness of the composite was enhanced and the elongation of the composite was almost twice that of the initial one. These changes were due to the dislocations and substructures stored in the Ti-43Al-9V alloy being decreased, the microstructure of the DsTi700 alloy turning to a duplex structure, the acicular α_2 phase being precipitated at the interfacial region and the residual stresses stored in interfacial region being eliminated. The precipitation of dual-scale silicides was the main reason for the slightly reduced strength. Compared with the initial composite, the tensile strength of the heat-treated composite at 25° and 700° only reduced by 2.7% and 4%, respectively. The primary annealing temperature had a huge impact on the mechanical properties of the composite. However, with the change in secondary annealing temperature, the mechanical properties of the composite were not changed significantly. After heat treatment at 940–960 °C/2 h/AC + 725–750 °C/6 h/AC, the composite might possess high, comprehensive mechanical properties.

Keywords: heat treatment; microstructure; mechanical properties; laminate composite

check for updates

Citation: Sun, W.; Cui, N.; Su, Y.; Zhang, S.; Xu, T.; Wang, X.; Kong, F. Effect of Heat Treatment on the Microstructure and Mechanical Properties of a Ti-TiAl Laminate Composite. *Metals* **2023**, *13*, 708. https://doi.org/10.3390/met13040708

Academic Editor: Emin Bayraktar

Received: 27 February 2023
Revised: 28 March 2023
Accepted: 3 April 2023
Published: 4 April 2023

Copyright: © 2023 by the authors. Licensee MDPI, Basel, Switzerland. This article is an open access article distributed under the terms and conditions of the Creative Commons Attribution (CC BY) license (https://creativecommons.org/licenses/by/4.0/).

1. Introduction

γ-TiAl alloy sheets have become a promising material for use in thermal protection shields due to their low density, high specific strength and excellent oxidation resistance [1–3]. However, their applications are hindered by poor room-temperature plasticity, poor fracture toughness and a narrow hot work window [4,5]. Recently, β-phase-containing TiAl alloys have been developed to overcome their limited hot deformability [6,7]. However, the ordered brittle B2 phase transformed from the β phase will further deteriorate the room-temperature plasticity and toughness of TiAl alloys [8,9]. Inspired by the shell structure, Ti-TiAl-based metal–intermetallic laminate (MIL) composites are expected to improve the fracture toughness of a TiAl intermetallic while maintaining its high strength. For example, at room temperature, the fracture toughness and ultimate tensile strength (UTS) of Ti-TiAl MIL composites fabricated via hot-pack rolling are 2.5–3.5 times and 1.2–1.5 times higher, respectively, than that of a monolithic TiAl alloy [10–12].

Although the toughness and strength of the composite are particularly high, the plasticity is not satisfactory. Previous studies [12,13] have shown that the plasticity of this kind of composite is not much higher than that of a monolithic TiAl alloy, and some are even lower. The reason for this phenomenon can be summarized as follows: (i) Due to the mismatch between the coefficient of thermal expansion of the titanium alloy and TiAl alloy, there will be a lot of residual stresses formed at the interfacial region. These residual stresses will cause delamination of the composite, thus decreasing the plasticity [14,15]. (ii) After hot rolling, there will be a large number of dislocations and substructures stored in

the composite, which may further decrease the plasticity of the composite [16,17]. (iii) The interfacial region is mainly composed of a brittle B2 phase and the microstructure of titanium alloy is a Widmannstatten structure, which is not conducive to the improvement of plasticity [18,19].

Heat treatment is an effective way to improve the mechanical properties of materials. Proper heat treatment can optimize the microstructure and release the residual stresses, which may solve the problems mentioned above. Moreover, investigating the influence of heat treatment on the microstructure and mechanical properties of a Ti-TiAl MIL composite is not only for scientific understanding but also for industrial applications. However, to the best of the authors' knowledge, the effect of heat treatment on the microstructure and its resultant impact on the mechanical properties of a Ti-TiAl MIL composite has not been reported to date.

The Ti-6Al-3Sn-10Zr- (Mo, Nb, W, Si) (wt.%) titanium alloy is a promising counterpart for a TiAl alloy, because its room-temperature tensile properties and fracture toughness are good. Moreover, compared with other titanium alloys, the high temperature tensile properties of this titanium alloy are excellent [20]. Therefore, in this paper, the Ti-6Al-3Sn-10Zr- (Mo, Nb, W, Si)/Ti-43Al-9V laminate composite was successfully fabricated via hot-pack rolling. The effect of heat treatment on the microstructure and mechanical properties of this composite was investigated. The purpose of this paper is to establish a heat-treatment process to improve the plasticity and fracture toughness of the composite without sacrificing the strength too much.

2. Materials and Methods

The Ti-TiAl MIL composite was fabricated using 3 pieces of as-forged Ti-6Al-3Sn-10Zr-(Mo, Nb, W, Si) (wt.%) (replaced by the DsTi700 alloy below) and 4 pieces of as-forged Ti-43Al-9V (at.%) (replaced by the TiAl alloy below). All pieces with a dimension of $70 \times 60 \times 2$ mm^3 were surface-polished and then alternately stacked to prepare a "sandwich". Next, the "sandwich" was hot pressed in a vacuum environment (10^{-2} Pa) at 1100 °C for 30 min under 30 MPa. Finally, the "sandwich" was sealed in a stainless-steel pack and hot-rolled at 1125 °C. The thickness reduction per pass was 10–30% and between each pass the sealed "sandwich" was kept at 1125 °C for 2–5 min. Finally, the as-rolled composite with a dimension of $200 \times 60 \times 2.3$ mm^3 was annealed at 590 °C for 1 h and then furnace cooled to room temperature. Some pieces were wire cut from the as-rolled composite and heat-treated according to Table 1. The primary heat treatment was used to reduce residual stress and regulate the content and morphology of the primary α phase and silicides. The secondary heat treatment was used to stabilize the microstructure of the titanium alloy, precipitate the α_2 phase at the interfacial region and regulate the morphology of secondary α phase.

Table 1. The heat-treatment process of the Ti-TiAl laminate composite.

No.	Primary Annealing	Secondary Annealing
HT1	920 °C/2 h/AC	725 °C/6 h/AC
HT2	940 °C/2 h/AC	700 °C/6 h/AC
HT3	940 °C/2 h/AC	725 °C/6 h/AC
HT4	940 °C/2 h/AC	750 °C/6 h/AC
HT5	960 °C/2 h/AC	725 °C/6 h/AC

The microstructure observation was performed using electron probe microanalysis (EPMA) equipped with energy dispersive X-ray spectrometry (EDS) and electron backscattered diffraction (EBSD). The volume fraction of a phase was measured using Image Pro Plus software. The 25 °C and 700 °C tensile tests were carried out along the rolling direction at a strain rate of 1.67×10^{-4} s^{-1} and 4.17×10^{-4} s^{-1}, respectively, and the dimension of gauge section was $5 \times 2 \times 20$ mm^3 (Figure 1a). According to ASTM E399-1990, the fracture toughness was evaluated using single edge-notched bend (SENB) samples at a

strain rate of 1.67×10^{-4} s^{-1}. The dimensions of the samples were $2 \times 1 \times 14$ mm^3 and $4 \times 2 \times 22$ mm^3 for arrester (AO) and divider orientation (DO), respectively (Figure 1b,c). The notch depth of the samples was 0.5 W (width of samples). The fracture toughness values (K_{IC}, MPa·$m^{1/2}$) were calculated using the following formula [21]:

$$K_{IC} = (PS/BW^{3/2}) f\ (a\ /\ W) \quad (1)$$

where P is the maximum load, S is the span, B is the thickness of specimens, W is the width of the specimens, a is the length of the notch and $f\ (a/W)$ is a geometrical function defined as

$$f\ (a/W) = \frac{3(a/W)^{1/2}[1.99\ -\ (a\ /\ W)(1\ -\ a/\ W)(2.15\ -\ 3.93a/W + 2.7(a\ /\ W)^2)]}{2(1 + 2a\ /\ W)(1\ -\ a/\ W)^{3/2}} \quad (2)$$

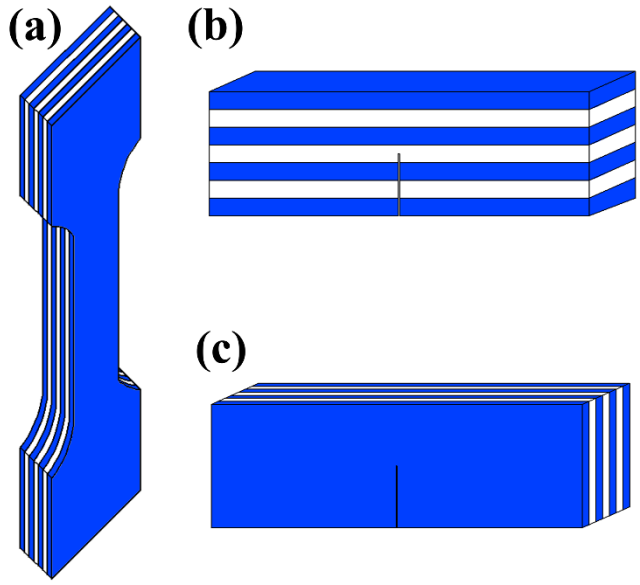


Figure 1. (**a**) Schematic diagram of tensile samples and fracture toughness samples in (**b**) arrester orientation and (**c**) divider orientation, respectively (Deep blue regions represent the TiAl alloy and white regions represent the DsTi700 alloy).

3. Results and Discussions

3.1. Microstructure Evolution

Figure 2 shows the microstructure of the initial and heat-treated composites. As is shown, the initial DsTi700 shows a Widmannstatten structure (Figure 2a). The initial TiAl alloy is composed of a γ phase elongated along the rolling direction and a B2 phase (Figure 2b). The initial interfacial region was 38 μm in thickness, composed of a fine acicular α_2 phase and B2 matrix (Figure 2c). The formation mechanism of the microstructure is similar to our previous study [18]. Figure 2d–f shows the microstructure of the heat-treated DsTi700 alloy. After heat treatment, the primary α phase is in lath and a large amount of silicides are precipitated from the β phase. With the increase in temperature, the content of the primary α phase decreases from 37.9 vol.% to 25.6 vol.%, but the content of silicides increases from 0.8 vol.% to 4.6 vol.% (Figure 2d–f). Moreover, with the increase in temperature, the silicides exhibit dual-scale and the size also gradually increase. Figure 2g–i shows the heat-treated microstructure of the interfacial region and the TiAl alloy. After heat treatment, the thickness of the interfacial region increased from 38 μm to 48–49 μm. With the increase in temperature, the acicular α_2 phase gradually became coarser. As for the TiAl alloy, the γ still elongated along the rolling direction, but the aspect ratio decreased.

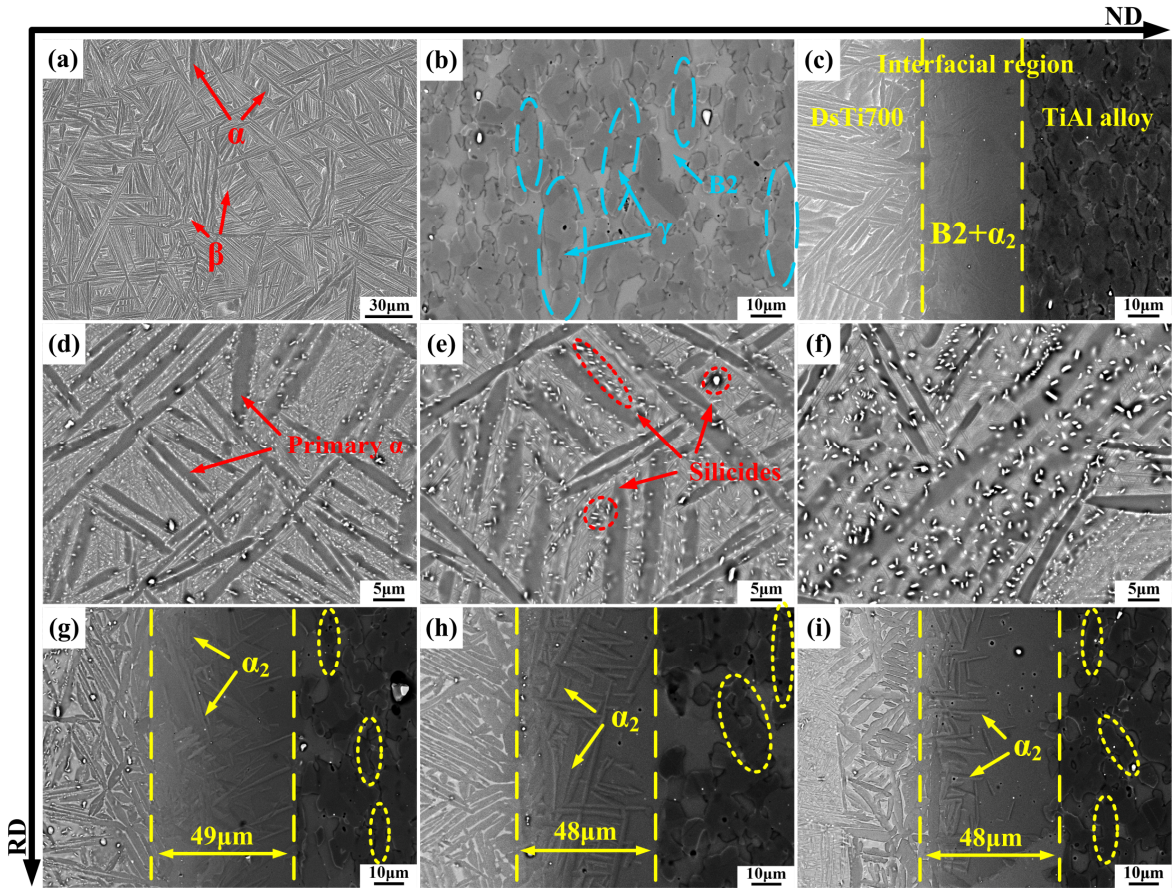
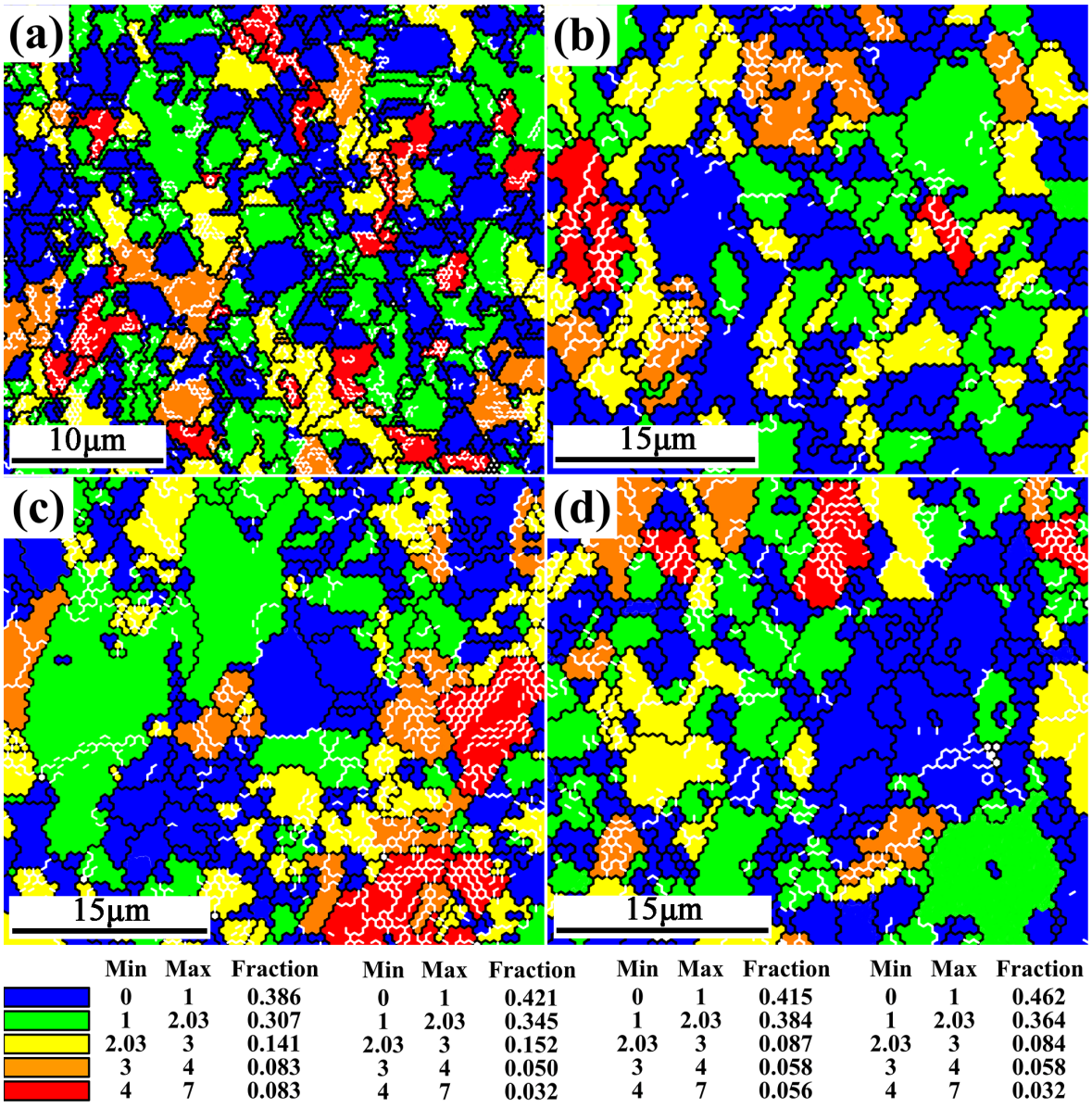


Figure 2. The cross-sectional microstructure of the initial and heat-treated composites: (**a**) DsTi700 alloy, (**b**) TiAl alloy and (**c**) interfacial region of initial composite; (**d**) DsTi700 alloy and (**g**) interfacial region of HT1; (**e**) DsTi700 alloy and (**h**) interfacial region of HT3, (**f**) DsTi700 alloy and (**i**) interfacial region of HT5.

Figure 3 shows the grain orientation spread (GOS) map of the initial and heat-treated TiAl alloy. GOS is defined as the average difference in orientation between the average misorientation and all measurements within one single grain. In other words, if the GOS value of a grain is high, there is a high dislocation density and severe lattice distortion. If the GOS value of a grain is low, this means there is low energy stored in this grain. As is shown in Figure 3, the blue and green areas represent the grain with a low GOS value and the yellow, orange and red areas represent the grain with a high GOS value. The white lines represent 2–15° grain boundaries and the black lines represent 15–180° grain boundaries. In the initial TiAl alloy, the volume fraction of grains with a high GOS value was 30.7% [13] (Figure 3a). After heat treatment, the volume fraction of the grains with a high GOS value decreased from 23.4% (yellow region + orange region + red region) to 17.4%, which means that when the heat treatment is at 920–960 °C, the dislocations, substructures and energy stored in the TiAl alloy are significantly reduced. The GOS analysis of the DsTi700 alloy is not shown in this article, because our previous study showed that after a 590 °C/1 h/FC heat treatment, the GOS value of the DsTi700 alloy was very low [13]. In this research, the GOS value of the DsTi700 alloy must be lower than our previous study. Therefore, the GOS value of the DsTi700 alloy is not shown in this article.



	Min	Max	Fraction	Min	Max	Fraction	Min	Max	Fraction	Min	Max	Fraction
	0	1	0.386	0	1	0.421	0	1	0.415	0	1	0.462
	1	2.03	0.307	1	2.03	0.345	1	2.03	0.384	1	2.03	0.364
	2.03	3	0.141	2.03	3	0.152	2.03	3	0.087	2.03	3	0.084
	3	4	0.083	3	4	0.050	3	4	0.058	3	4	0.058
	4	7	0.083	4	7	0.032	4	7	0.056	4	7	0.032

Figure 3. GOS analysis of the initial and heat-treated TiAl alloy: (**a**) initial TiAl alloy [13], (**b**) HT1, (**c**) HT3 and (**d**) HT5.

Figure 4 shows the kernel average misorientation (KAM) map of the initial and heat-treated interfacial regions. KAM is defined as the average misorientation between a kernel point and its neighboring points which exclude the grain boundary. Generally speaking, it reflects the local lattice curvature and residual stresses. For a defect-free interfacial region, if the KAM value is low, the residual stress stored in the interfacial region is low, which indicates a high bonding strength between a titanium alloy and a TiAl alloy. As shown in Figure 4, after heat treatment, the KAM value significantly decreased, which indicates that the heat-treatment process can eliminate the interfacial residual stress of composite. In addition, the KAM value of HT1 and HT5 is very similar, which means that the interfacial residual stresses of the composite can be eliminated when the heat-treatment temperature and time exceed 920 °C and 2 h.

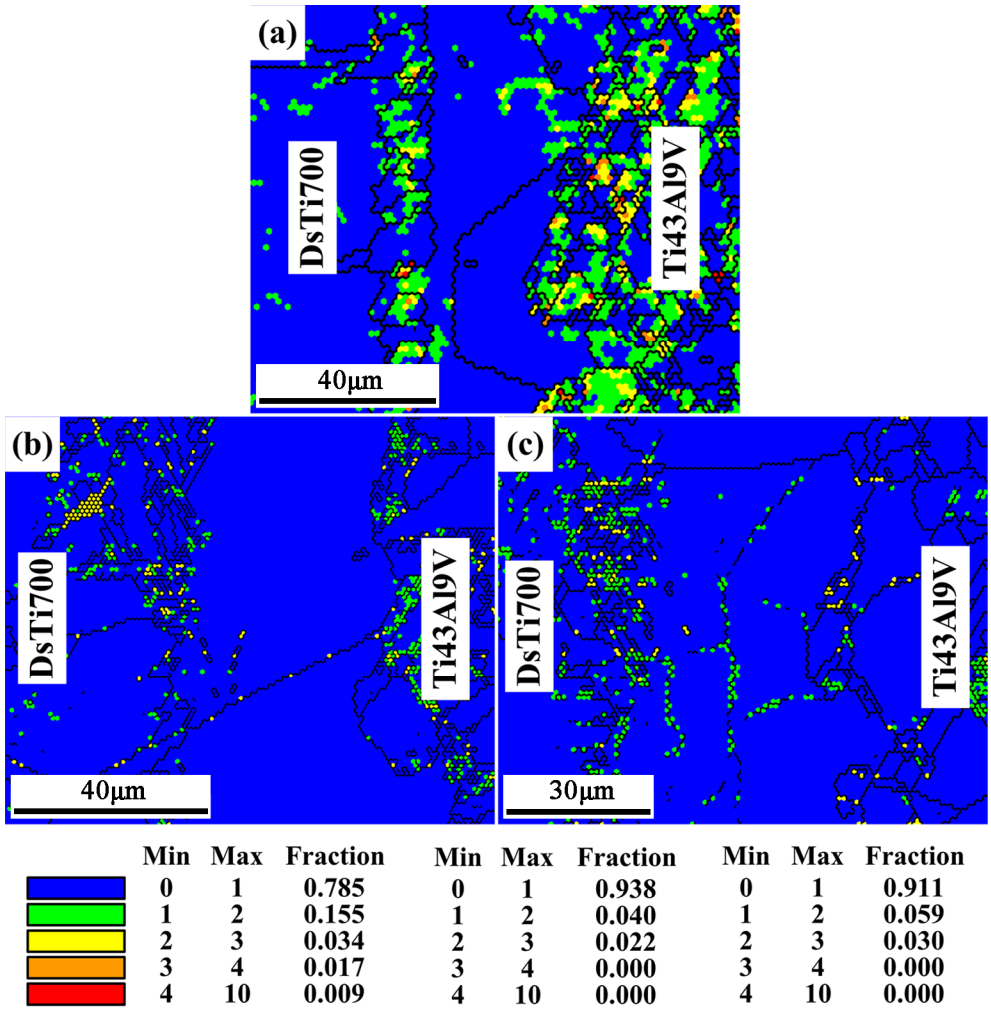


Figure 4. KAM analysis of the initial and heat-treated interfacial regions: (**a**) initial interfacial region, (**b**) HT1 and (**c**) HT5.

Figure 5 shows the microstructure of heat-treated composites with a different secondary annealing process. As shown in Figure 5a–c, with the increase in temperature, the content of the secondary α phase and silicides do not change obviously. However, the morphology of the secondary α phase changes from fine acicular to lath, and finally forms a lamella structure. Figure 5d–f illustrates that after secondary annealing, the thickness of the interfacial region is nearly unchanged. However, a large amount of acicular α_2 phase is precipitated from the B2 matrix. It is necessary to point out that there is no obvious change in the microstructure of the TiAl alloy at 700–750 °C. Therefore, in this article, we do not discuss the microstructure evolution of the TiAl alloy after secondary annealing.

3.2. Tensile Properties

Figure 6 and Table 2 show the 25 °C and 700 °C tensile properties of initial and heat-treated composites. At 25 °C, the Young modulus (E), ultimate tensile strength (UTS) and elongation (E.L.) of initial composite were 140.2 GPa, 876 MPa and 1.1%, respectively. After heat treatment, the E of the composites were nearly unchanged, which indicates that heat treatment has little effect on the E of composites. The HT3 composite had the highest UTS 852 MPa and E.L. 2.0%. This means that heat treatment can significantly improve the room-temperature plasticity of a composite (nearly two times that of the initial composite) without sacrificing strength too much (reduced by 2.7%). For the heat-treated composite, with the increase in primary annealing temperature, the UTS exhibited a trend of first increasing and then decreasing, but E.L. continuously increased. However, the secondary

annealing temperature has little effect on the UTS and E.L. of a composite. The variation trend of tensile properties at 700 °C is similar to the tensile properties at 25 °C. The reasons for these phenomena can be explained by the microstructure and fracture morphology of composites, which will be discussed below.

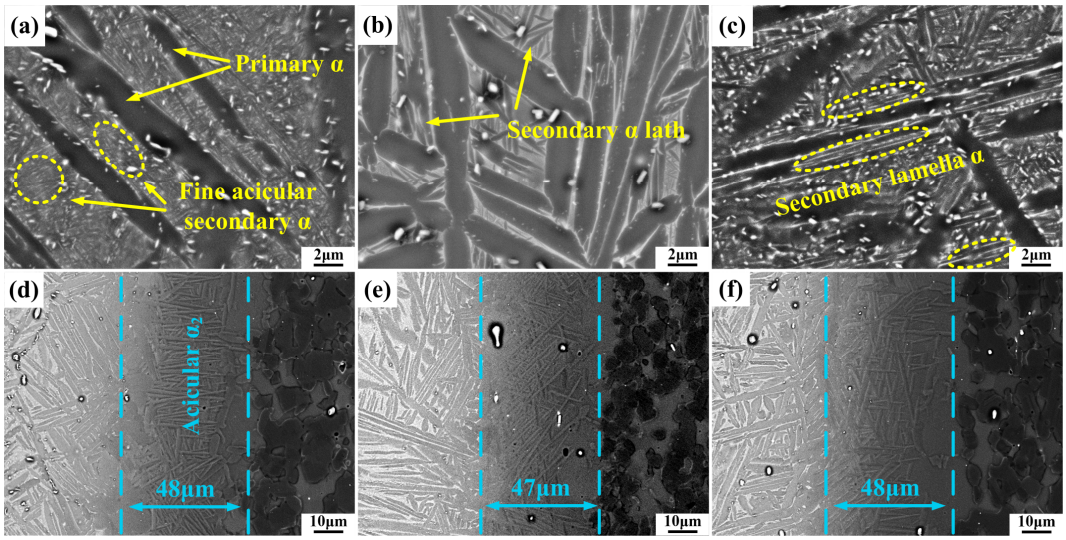


Figure 5. The microstructure of heat-treated composites: (**a**) DsTi700 alloy and (**d**) interfacial region of HT2; (**b**) DsTi700 alloy and (**e**) interfacial region of HT3; (**c**) DsTi700 alloy and (**f**) interfacial region of HT4.

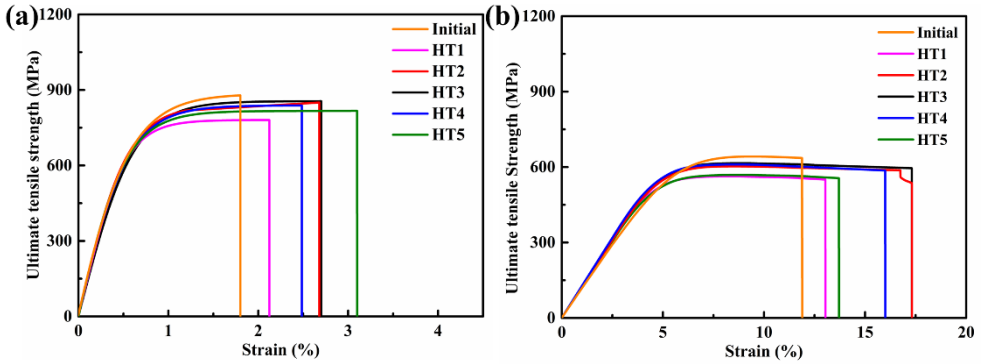


Figure 6. 25 °C and 700 °C tensile properties of initial and heat-treated composites: (**a**) 25 °C tensile properties and (**b**) 700 °C tensile properties.

Table 2. Tensile properties of initial and heat-treated composites.

NO.	25 °C Tensile Properties		700 °C Tensile Properties	
	UTS (MPa)	E.L. (%)	UTS (MPa)	E.L. (%)
HT1	785	1.4	563	8.6
HT2	850	2.0	603	12.4
HT3	852	2.0	615	12.9
HT4	846	1.9	610	11.6
HT5	816	2.1	569	13.3
Initial	876	1.1	641	7.5

Figure 7 shows the fracture morphology of the 25 °C tensile test composites. The macroscopic fracture morphology of the initial composite shows that the fracture surface of the DsTi700 alloy is a plane, which indicates that the plasticity of the initial DsTi700 is poor (Figure 7a). Moreover, the delamination phenomenon is observed in the initial

composite, which may further decrease the plasticity of the composite. After heat treatment, the fracture surface of the composite becomes stepped and the DsTi700 alloy is fractured in shear mode, which suggests the enhancement of the DsTi700 alloy (Figure 7b). Additionally, the delamination phenomenon cannot be observed in the heat-treated composite.

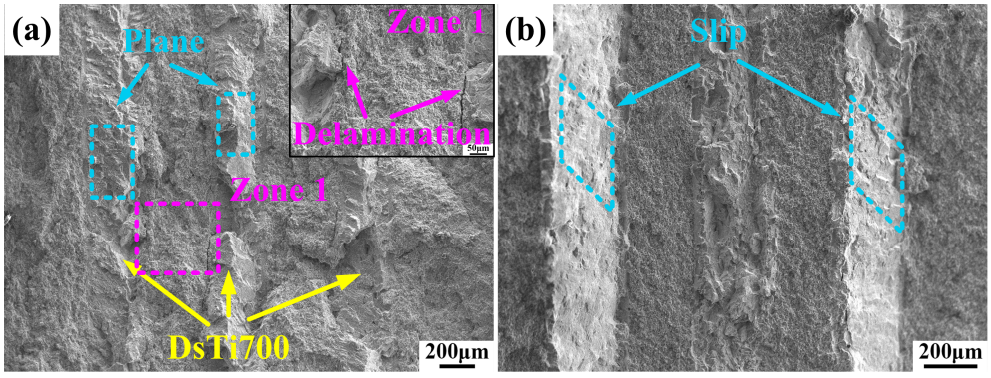


Figure 7. 25 °C macroscopic fracture morphology of the initial and heat-treated composites: (**a**) initial composite and (**b**) HT3.

Figure 8 shows the 25 °C fracture morphology of the initial and heat-treated DsTi700 alloy. Figure 8a shows that the initial DsTi700 alloy exhibits a brittle fracture and a lamella α phase can be observed. With the increase in primary annealing temperature, the content of dimples gradually increased. When the temperature reached 960 °C, the DsTi700 alloy was completely transformed into ductile fractures.

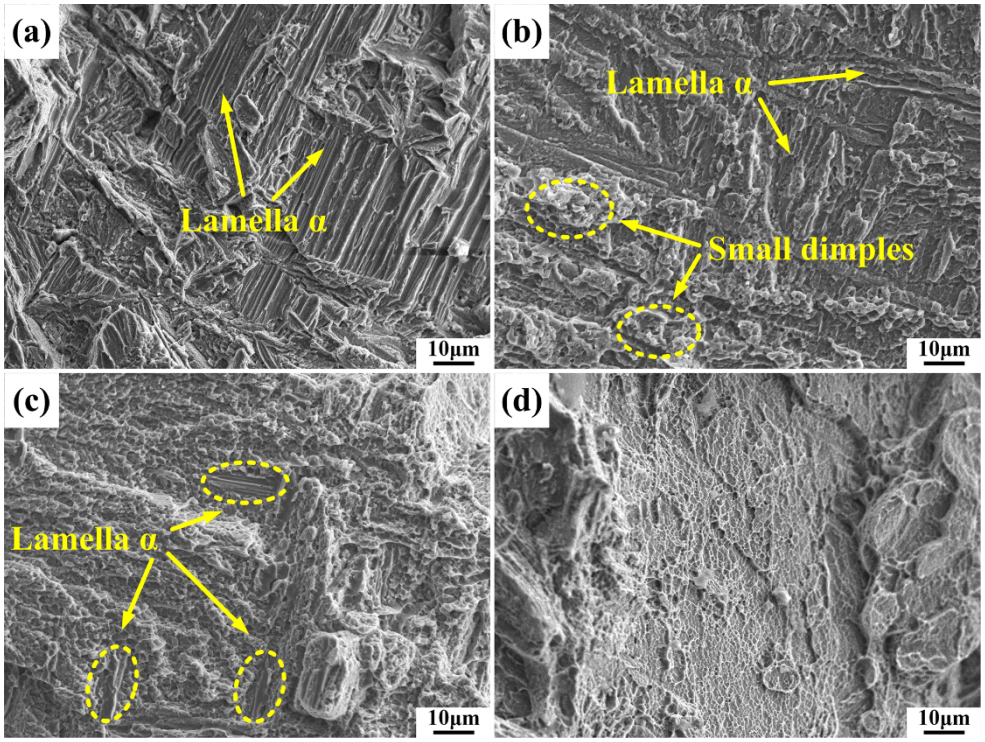


Figure 8. 25 °C fracture morphology of the initial and heat-treated DsTi700 alloy: (**a**) initial composite, (**b**) HT1, (**c**) HT3 and (**d**) HT5.

Figure 9 is the 25 °C fracture morphology of the initial and heat-treated TiAl alloy and the interfacial regions. Figure 9a,b shows that both the initial and heat-treated TiAl alloy exhibit brittle transgranular fractures. This demonstrates that although heat treatment can decrease the GOS value of a TiAl alloy, it cannot change the fracture mode of the TiAl alloy.

The initial interfacial region exhibits cleavage fractures (Figure 9c), but the HT3 composite exhibits quasi-cleavage fractures (Figure 9d). This means that heat treatment can soften the interfacial region, reduce its residual stresses and change its fracture mode.

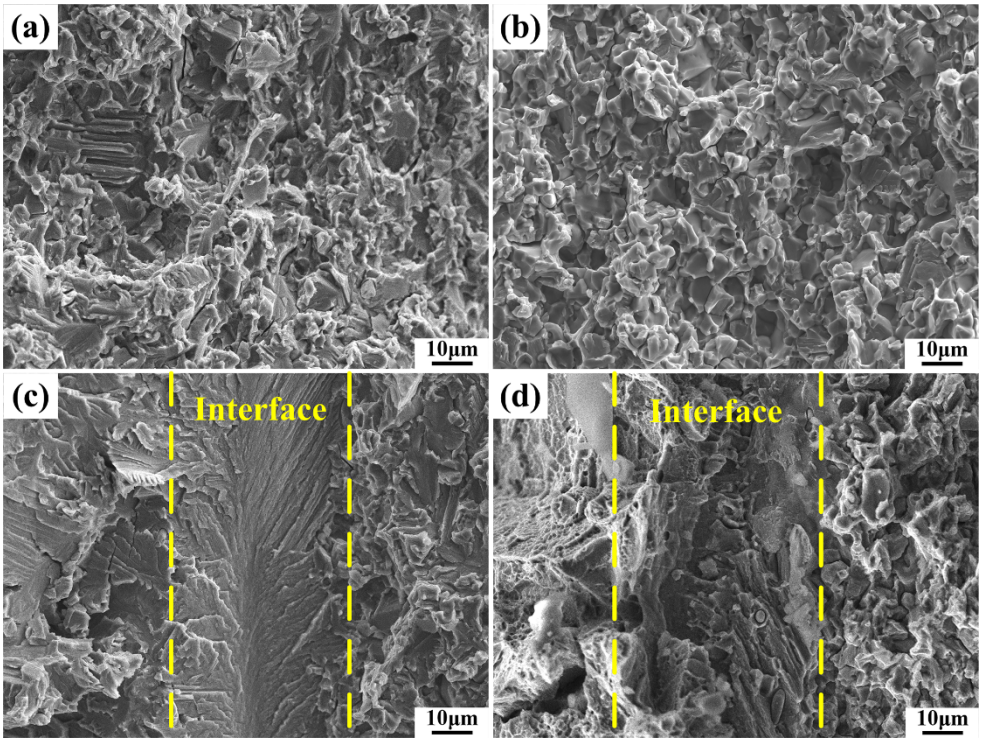


Figure 9. 25 °C fracture morphology of the initial and heat-treated TiAl alloy and interfacial region: (**a**) TiAl alloy and (**c**) interfacial region of initial composite; (**b**) TiAl alloy and (**d**) interfacial region of HT3.

Based on the evidence mentioned above, the reason that the heat-treated composites possess both high strength and plasticity at 25 °C can be summarized as follows: (i) After heat treatment, the GOS value of the TiAl alloy significantly decreased (Figure 3), which means that the dislocations, substructures and energy stored in the TiAl alloy are reduced [22,23]. Therefore, the plasticity of the TiAl alloy and composites must be improved. (ii) In a titanium alloy, the widmannstatten structure always shows the highest strength and the lowest plasticity. After heat treatment, the composite exhibits a duplex microstructure, which has the best comprehensive mechanical properties among the four typical microstructures of titanium alloys [24,25]. Therefore, the plasticity of the composite is improved. (iii) The KAM value of the heat-treated interfacial region is much lower than that of the initial one (Figure 4). This indicates that the bonding strength between the DsTi700 and TiAl alloy is enhanced. The improved bonding strength can avoid the delamination phenomenon, thus improving the plasticity of composites [26,27]. (iv) After secondary annealing, there is a large number of α_2 phase precipitated from the B2 phase at the interfacial region (Figure 5). In Ti-Al-based intermetallics, the plasticity of the α_2 phase is higher than the B2 phase. Therefore, the fracture mode of the interfacial region changes from cleavage fractures to quasi-cleavage fractures (Figure 9), which may further increase the plasticity of a composite. (v) Figure 2d–f shows that after primary annealing, the dual-scale silicides are precipitated from the DsTi700 alloy and these dual-scale silicides are beneficial for the enhancement of strength [20,28]. Therefore, after heat treatment, although the plasticity of a composite is much improved, the composite still maintains a high strength.

With the increase in primary annealing temperature, the UTS of composites shows a trend of first increasing and then decreasing. When the primary annealing temperature

increases from 920 °C to 940 °C, the content of silicides and secondary α phase is increased. Dislocation movement is hindered by silicides and the secondary α phase, thus improving the UTS of composites. When the annealing temperature comes to 960 °C, the content of silicides and secondary α phase is still increased. However, the increase in silicides is not because of their increasing quantity but increasing size. According to the Orowan strengthening mechanism [29,30], large size silicides may weaken a strengthening effect, thus decreasing the UTS of a composite. Moreover, the increase in silicides may weaken solid solution strengthening, which may further decrease the UTS of a composite. With the increase in secondary annealing temperature, the UTS and E.L. of the composite was nearly unchanged. It is because of the content of silicides, the content of secondary α phase, the dislocations and substructures stored in the TiAl alloy and the residual stresses and phase composition of the interfacial region are not dependent on the secondary annealing temperature. Therefore, the tensile properties of a composite are not sensitive to changes in secondary annealing temperature.

At 700 °C, the strength of the initial composite is higher than that of the heat-treated composite. It is due to the fact that (i) after heat treatment, the GOS value of the TiAl alloy significantly decreased. Thus, the strength of the composite may decrease. (ii) The strength of the α_2 phase at high temperature is lower than the B2 phase. Therefore, the precipitated α_2 phase may decrease the strength of the composite. With the increase in primary annealing temperature, the UTS of composites shows a trend of first increasing and then decreasing. This may be due to the fact that from 920–940 °C, the dual-scale silicides and secondary α phase can increase the strength of composite. However, from 940–960 °C, the low GOS value can decrease the strength of composite. Moreover, the increase in silicides may weaken solid solution strengthening, which may further decrease the strength of a composite.

3.3. Fracture Toughness

Table 3 shows the fracture toughness of initial and heat-treated composites. The HT5 composite exhibits the highest fracture toughness, with values of 34.7 MPa·$m^{1/2}$ and 31.9 MPa·$m^{1/2}$ for arrester orientation (AO) and divider orientation (DO), respectively. However, the HT1 composite shows the lowest fracture toughness which is lower than the initial composite. With the increase in primary and secondary annealing temperature, the fracture toughness of composites in two directions gradually increased. Compared with the initial composite, the fracture toughness of heat-treated composites showed no significant changes. These phenomena can be explained by the crack propagation features of the composites.

Table 3. Fracture toughness of the initial and heat-treated composites.

NO.	K_{IC} (MPa·$m^{1/2}$)	
	AO	DO
HT1	18.7	15.2
HT2	31.3	29.6
HT3	32.8	30.8
HT4	33.4	30.6
HT5	34.7	31.9
Initial	31.4	29.3

Figure 10 is the crack propagation features of the initial and heat-treated composites in AO. Figure 10a shows that the crack started in the DsTi700 alloy then passed through the TiAl alloy in a straight line. When the crack propagates to the next layer of the DsTi700 alloy, crack deflection, bridging and plastic deformation can be observed. However, for the HT1 composite (Figure 10b), the crack propagates forward in a straight line, which indicates the low fracture toughness of the HT1 composite. For the HT3 composite, crack deflection and bridging are observed at the interfacial region and in the DsTi700 alloy, respectively.

Moreover, the magnified area in zone 1 (Figure 10e) shows that crack deflection is observed at the acicular α_2 phase in the interfacial region (marked with the blue dashed lines). This illustrates that the precipitated α_2 phase is beneficial for the improvement of fracture toughness. For the HT5 composite (Figure 10d), besides crack deflection and bridging, plastic deformation is also observed in the DsTi700 alloy (Figure 10f).

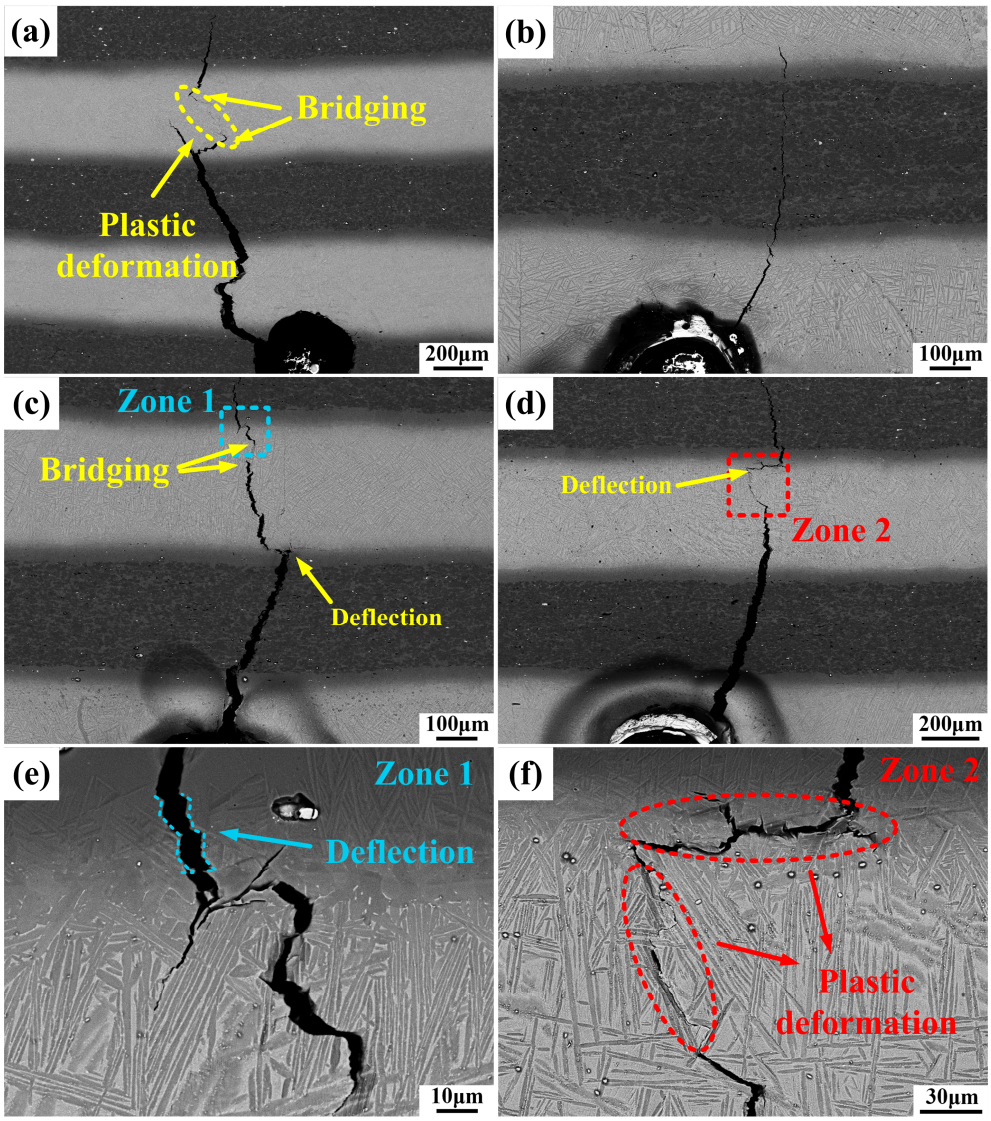


Figure 10. Crack propagation features of the initial and heat-treated composites: (**a**) initial composite, (**b**) HT1, (**c**) HT3, (**d**) HT5 and (**e**,**f**) magnified areas of picture (**c**,**d**), respectively.

Figure 11 shows the crack propagation features of the initial and heat-treated composites in the DO. Figure 11a shows that in the DO, the fracture morphology of the initial DsTi700 alloy is rugged. This means that the crack propagation is resisted by the DsTi700 alloy. In Figure 11b, the fracture morphology of the DsTi700 is a plane, which indicates that the resistance against crack propagation is reduced. For the HT3 composite (Figure 11c), the DsTi700 alloy is fractured in shear mode and the delamination phenomenon is observed between the DsTi700 alloy and interfacial region. The A.A. Griffith model shows that the critical stress of the crack tip can be reduced by the elongated crack [31]:

$$\sigma_C = [E \cdot (Y + Yp)/(\pi \cdot C)]^{1/2} \quad (3)$$

where σ_C is the critical stress of the crack tip and C is the length of the crack propagation. E is the Young modulus of material, Y and Yp are the constants of fracture surface energy. Therefore, the fracture toughness of the composite can be enhanced by the delamination phenomenon. In the HT5 composite (Figure 11d), the convolution phenomenon [32] is shown in the TiAl alloy, which illustrates that the fracture toughness of the composite is further enhanced.

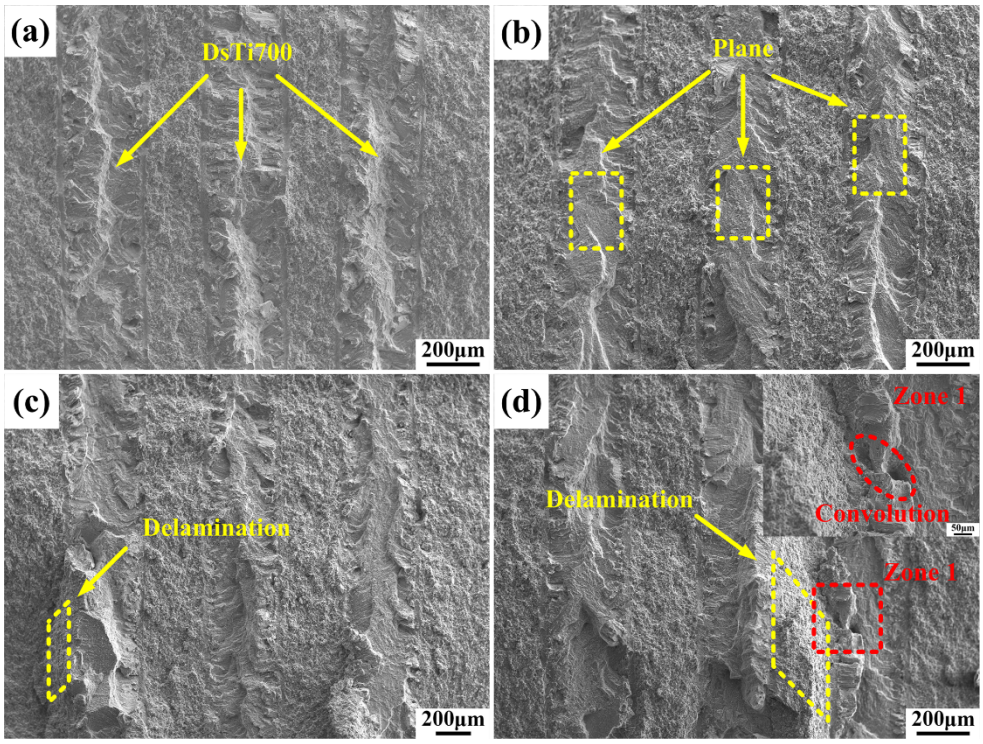


Figure 11. Fracture morphology of the initial and heat-treated composites tested in divider orientation: (**a**) initial composite, (**b**) HT1, (**c**) HT3 and (**d**) HT5.

Based on the analysis mentioned above, the enhancement of fracture toughness of heat-treated composites can be explained as follows: (i) After heat treatment, the dislocations and substructures stored in the TiAl alloy are significantly decreased, which may increase crack propagation resistance, thus improving the fracture toughness of composites. (ii) The crack is deflected by the α_2 phase precipitated at the interfacial region, which increases the length of a crack and reduces the driving force of crack propagation [31].

With the increase in primary annealing and secondary annealing temperature, this is due to the fact that (i) with the increase in primary annealing temperature, the dislocations and substructures stored in the TiAl alloy are decreased. (ii) With the increase in primary annealing temperature, the content of the secondary α phase in the DsTi700 alloy is gradually increased. Compared with the primary α phase, the secondary α phase has a more positive effect on the improvement of fracture toughness in a duplex structure. (iii) Figure 2g–i indicates that the width of the precipitated α_2 phase is gradually increased, which may further increase the fracture toughness of the composite. (iv) With the increase in secondary annealing temperature, the secondary α phase is gradually changed from an acicular to lamellar structure (Figure 5a–c). The lamellar structure is more beneficial for the enhancement of fracture toughness [33].

As showed in Table 3, heat treatment has little effect on the fracture toughness of a composite. It is due to that fact that the initial titanium alloy is a Widmannstatten structure, but after heat treatment, the titanium alloy exhibits a duplex microstructure. The K_{IC} value of the titanium alloy with a Widmannstatten structure is always higher than a titanium alloy with a duplex microstructure. Thus, this may decrease the K_{IC} value of a composite. However, after heat treatment, the residual stress stored in the TiAl alloy is decreased and

a lot of acicular α_2 phase precipitates from the brittle B2 phase at the interfacial region. These may increase the resistance against crack propagation and thus increase the K_{IC} value of the composite. In this case, the fracture toughness of the composite does not change significantly.

Combining Tables 2 and 3, the HT1 composite shows the lowest mechanical properties. The fracture toughness of the HT1 composite is even lower than the initial composite. The HT2, HT3 and HT4 composites show similar mechanical properties. However, among these three composites, the HT3 composite shows the highest tensile properties and good fracture toughness. The E.L. and fracture toughness of the HT5 composite are a little bit higher than the HT3 composite. However, the UTS of the HT5 composite is much lower than the HT3 composite. Thus, among these five composites, the HT3 composite shows the optimal comprehensive mechanical properties. Table 4 is a comparison of the tensile properties and fracture toughness of the HT3 composite with the Ti-43Al-9V alloy and other kinds of Ti-Al-based laminate composites. As is shown, compared with the monolithic Ti-43Al-9V alloy, the HT3 composite shows excellent 25 °C tensile properties and fracture toughness. The E.L. and fracture toughness are promoted by 43% and 98%, respectively. The Ti-(Ti/Al) composite shows outstanding fracture toughness and good E.L. However, the UTS is much lower than the HT3 composite. Compared with other composites, the HT3 composite also shows excellent mechanical properties.

Table 4. Comparison of HT3 composite with the Ti-43Al-9V alloy and other kinds of Ti-Al-based laminate composite.

Composites	25 °C Tensile Properties		700 °C (750 °C) Tensile Properties		K_{IC} (MPa·m$^{1/2}$)	
	UTS (MPa)	E.L. (%)	UTS (MPa)	E.L. (%)	AO	DO
HT3	852	2.0	615	12.9	32.8	30.8
(TiB/Ti)-TiAl [34]	-	-	469	-	30.9	-
(TiB/Ti)-Ti_3Al [35,36]	641	-	433	-	25.8	21.4
Ti-TiAl [37]	654	0.3 [a]	418	1.0 [a]	31.4	26.6
Ti-(Ti/Al) [38]	606	1.6 [a]	-	-	47.6	-
TiAl/Ti_2AlNb [39]	812	0.45 [a]	539 [b]	5.8 [a,b]	30.8	26.4
Ti-43Al-9V [7]	826	1.4	671	27	16.6	

[a] Data obtained from the figure. [b] Properties tested at 750 °C.

4. Conclusions

Based on the original data and analysis presented above, several conclusions can be made which are as follows:

(1) The plasticity and fracture toughness of composites are successfully enhanced by heat treatment without sacrificing strength too much. The E.L. of the HT3 composite is nearly two times higher than the initial one. Meanwhile, the UTS of the HT3 composite is only reduced by 2.7%.

(2) With the increase in primary annealing temperature, the UTS of composites shows a tendency to first increase and then decrease, but E.L. continuously increased. The secondary annealing temperature has less influence on the UTS and E.L. of composites. The fracture toughness of composites in two directions is enhanced with the increase in primary and secondary annealing temperature.

(3) The decrease in dislocations, substructures and residual stresses stored in the TiAl alloy and interfacial region, as well as the acicular α_2 phase precipitated at the interfacial region, are the main reasons for plasticity improvement. The strength of composites is enhanced by precipitated dual-scale silicides.

(4) After heat treatment at 940–960 °C/2 h/AC + 725–750 °C/6 h/AC, the composite may possess a high, comprehensive mechanical property. In this study, the HT3 composite possesses the optimal comprehensive mechanical properties. The UTS and E.L. at 25 °C

and 700 °C are 852 MPa and 2.0% and 615 MPa and 12.9%, respectively. The fracture toughness in the AO and DO are 32.8 MPa·$m^{1/2}$ and 30.8 MPa·$m^{1/2}$, respectively.

Author Contributions: Conceptualization, W.S. and F.K.; methodology, W.S.; software, S.Z.; validation, T.X. and X.W.; formal analysis, Y.S.; investigation, W.S.; resources, W.S. and F.K.; data curation, S.Z.; writing—original draft preparation, W.S.; writing—review and editing, W.S., N.C. and X.W.; visualization, T.X.; supervision, W.S.; project administration, W.S., N.C., Y.S. and F.K.; funding acquisition, W.S., N.C., Y.S. and F.K. All authors have read and agreed to the published version of the manuscript.

Funding: This work was financially supported by the National Natural Science Foundation of China (52201126, 51471056, 51704174), the Natural Science Foundation of Shandong Province, China (ZR2022QE067), the Shandong Province Key Research and Development Program (2019GGX102045) and the China scholarship Council (201708330547).

Institutional Review Board Statement: Not applicable.

Informed Consent Statement: Not applicable.

Data Availability Statement: The data would be available if requested.

Conflicts of Interest: The authors declare that they have no known competing financial interests or personal relationships that could have appeared to influence the work reported in this paper.

References

1. Ding, J.; Zhang, M.; Liang, Y.; Ren, Y.; Dong, C.; Lin, J. Enhanced high-temperature tensile property by gradient twin structure of duplex high-Nb-containing TiAl alloy. *Acta Mater.* **2018**, *161*, 1–11. [CrossRef]
2. Erdely, P.; Staron, P.; Maawad, E.; Schell, N.; Clemens, H.; Mayer, S. Lattice and phase strain evolution during tensile loading of an intermetallic, multi-phase γ-TiAl based alloy. *Acta Mater.* **2018**, *158*, 193–205. [CrossRef]
3. Zhu, B.; Xue, X.Y.; Kou, H.C.; Li, X.L.; Li, J.S. Effect of microstructure on the fracture toughness of multi-phase high Nb-containing TiAl alloys. *Intermetallics* **2018**, *100*, 142–150. [CrossRef]
4. Kim, J.Y.; Park, E.S.; Lee, T.; Ryu, S.; Kim, S.E.; Kim, S.W. Origin of enhanced room temperature ductility in TiAl alloys: Reducing activation difference of deformation mechanism of γ phase. *J. Alloys Compd.* **2022**, *899*, 163307. [CrossRef]
5. Cui, S.; Cui, C.X.; Yang, S.C.; Liu, S.J. Microstructure and mechanical properties of hybrid in-situ Ti_2AlCw/Mo_2B_5p reinforced TiAl alloy. *Mater. Sci. Eng. A* **2022**, *829*, 142182. [CrossRef]
6. Cui, N.; Wu, Q.; Bi, K.; Wang, J.; Xu, T.; Kong, F. Effect of multi-directional forging on the microstructure and mechanical properties of β-solidifying TiAl alloy. *Materials* **2019**, *12*, 1381. [CrossRef] [PubMed]
7. Zhang, Y.; Wang, X.; Kong, F.; Sun, L.; Chen, Y. A high-performance β-solidifying TiAl alloy sheet: Multi-type lamellar microstructure and phase transformation. *Mater. Charact.* **2018**, *138*, 136–144. [CrossRef]
8. Narayana, P.L.; Li, C.-L.; Kim, S.-W.; Kim, S.-E.; Marquardt, A.; Leyens, C.; Reddy, N.S.; Yeom, J.-T.; Hong, J.-K. High strength and ductility of electron beam melted β stabilized γ-TiAl alloy at 800 °C. *Mater. Sci. Eng. A* **2019**, *756*, 41–45. [CrossRef]
9. Liu, Y.; Li, J.; Tang, B.; Wang, W.Y.; Lai, M.; Zhu, L.; Kou, H. Formation mechanism of γ twins in β-solidified γ-TiAl alloys. *J. Mater. Sci. Technol.* **2022**, *105*, 164–171. [CrossRef]
10. Sun, W.; You, F.H.; Kong, F.T.; Wang, X.P.; Chen, Y.Y. Effect of residual stresses on the mechanical properties of Ti-TiAl laminate composites fabricated by hot-pack rolling. *Mater. Charact.* **2020**, *166*, 110394. [CrossRef]
11. Sun, W.; Fan, H.; You, F.; Kong, F.; Wang, X.; Chen, Y. Prediction of interfacial phase formation and mechanical properties of Ti6Al4V–Ti43Al9V laminate composites. *Mater. Sci. Eng. A* **2020**, *782*, 139173. [CrossRef]
12. Sun, W.; You, F.; Kong, F.; Wang, X.; Chen, Y. Fracture mechanism of a high tensile strength and fracture toughness Ti6Al4V–TiAl laminated composite. *J. Alloys Compd.* **2020**, *820*, 153088. [CrossRef]
13. Sun, W.; You, F.; Kong, F.; Wang, X.; Chen, Y. Enhanced tensile strength and fracture toughness of a Ti-TiAl metal-intermetallic laminate (MIL) composite. *Intermetallics* **2020**, *118*, 106684. [CrossRef]
14. Bermejo, R.; Torres, Y.; Sanchez-Herencia, A.J.; Baudin, C.; Anglada, M.; Llanes, L. Residual stresses, strength and toughness of laminates with different layer thickness ratios. *Acta Mater.* **2006**, *54*, 4745–4757. [CrossRef]
15. Yuan, M.; Wang, Z.; Yao, Y.; Li, L. Finite element analysis of thermal stresses in Ti-Al_3Ti metal-intermetallic laminated composites. *Results Phys.* **2019**, *15*, 102706. [CrossRef]
16. Zhou, H.T.; Kong, F.T.; Wu, K.; Wang, X.P.; Chen, Y.Y. Hot pack rolling nearly lamellar Ti-44Al-8Nb-(W, B, Y) alloy with different rolling reductions: Lamellar colonies evolution and tensile properties. *Mater. Des.* **2017**, *121*, 202–212. [CrossRef]
17. Li, T.R.; Liu, G.H.; Xu, M.; Wang, B.X.; Niu, H.Z.; Misra, R.D.K.; Wang, Z.D. Effects of hot-pack rolling process on microstructure, high-temperature tensile properties, and deformation mechanisms in hot-pack rolled thin Ti–44Al–5Nb-(Mo, V, B) sheets. *Mater. Sci. Eng. A* **2019**, *764*, 138197. [CrossRef]
18. Sun, W.; Yang, F.; Kong, F.; Wang, X.; Chen, Y. Interface characteristics of Ti6Al4V-TiAl metal-intermetallic laminate (MIL) composites prepared by a novel hot-pack rolling. *Mater. Charact.* **2018**, *144*, 173–181. [CrossRef]

19. Wang, X.R.; Yang, Y.Q.; Luo, X.; Zhang, W.; Zhao, G.M.; Huang, B. An investigation of Ti-43Al-9V/Ti-6Al-4V interface by diffusion bonding. *Intermetallics* **2013**, *36*, 127–132. [CrossRef]
20. Su, Y.; Fan, H.; You, F.; Kong, F.; Wang, X.; Chen, Y. Improved tensile properties of a novel near-α titanium alloy via tailoring microstructure by hot-rolling. *Mater. Sci. Eng. A* **2020**, *790*, 139588. [CrossRef]
21. Tian, Y.; Wang, E.H.; Li, W.; Niu, Z.Y.; Chang, Y.P.; Guo, C.H.; Wang, Z.Q.; Leng, Z.; Jiang, F.C. Improved fracture toughness of NiTi shape memory alloy fiber-reinforced Ti-Al metal-intermetallic-laminate composite. *J. Alloys Compd.* **2018**, *739*, 669–677. [CrossRef]
22. Chen, X.F.; Tang, B.; Liu, D.; Wei, B.B.; Zhu, L.; Liu, R.C.; Kou, H.C.; Li, J.S. Dynamic recrystallization and hot processing map of Ti-48Al-2Cr-2Nb alloy during the hot deformation. *Mater. Charact.* **2021**, *179*, 111332. [CrossRef]
23. Singh, V.; Mondal, C.; Sarkar, R.; Bhattacharjee, P.P.; Ghosal, P. Dynamic recrystallization of a β(B2)-Stabilized γ-TiAl based Ti–45Al–8Nb–2Cr-0.2B alloy: The contributions of constituent phases and Zener-Hollomon parameter modulated recrystallization mechanisms. *J. Alloys Compd.* **2020**, *828*, 154386. [CrossRef]
24. Jia, R.; Zeng, W.; Zhao, Z.; Zhang, P.; Xu, J.; Wang, Q. In-situ investigation on the deformation mechanism of duplex microstructure of a near α titanium alloy. *J. Alloys Compd.* **2022**, *893*, 162184. [CrossRef]
25. Ma, Y.; Youssef, S.S.; Feng, X.; Wang, H.; Huang, S.; Qiu, J.; Lei, J.; Yang, R. Fatigue crack tip plastic zone of α + β titanium alloy with Widmanstatten microstructure. *J. Mater. Sci Technol.* **2018**, *34*, 2107–2115. [CrossRef]
26. Nambu, S.; Michiuchi, M.; Inoue, J.; Koseki, T. Effect of interfacial bonding strength on tensile ductility of multilayered steel composites. *Compos. Sci. Technol.* **2009**, *69*, 1936–1941. [CrossRef]
27. Zhang, Y.J.; Cheng, X.W.; Cai, H.N.; Zhang, H.M. Effects of annealing time on the microstructures and tensile properties of formed laminated composites in Ti-Ni system. *J. Alloys Compd.* **2017**, *699*, 695–705. [CrossRef]
28. Wang, S.; An, Q.; Zhang, R.; Jiang, S.; Huang, L.J.; Chen, R.; Liu, B.X.; Jiao, Y.; Geng, L. Microstructure characteristics and enhanced properties of network-structured TiB/(TA15-Si) composites via rolling deformation at different temperatures. *Mater. Sci. Eng. A* **2022**, *829*, 142176. [CrossRef]
29. Xu, S.; Zhou, Z.; Long, F.; Jia, H.; Guo, N.; Yao, Z.; Daymond, M.R. Combination of back stress strengthening and Orowan strengthening in bimodal structured Fe–9Cr–Al ODS steel with high Al addition. *Mater. Sci. Eng. A* **2019**, *739*, 45–52. [CrossRef]
30. Dieter, G.E.; Bacon, D.J. *Mechanical Metallurgy*; McGraw-hill: New York, NY, USA, 1976.
31. Griffith, A. The phenomena of rupture and flow in solid. *Philos. Trans. R Soc. A Math. Phys. Eng. Sci.* **1920**, *221*, 163–198.
32. Lesuer, D.R.; Syn, C.K.; Sherby, O.D.; Wadsworth, J.; Lewandowski, J.J.; Hunt, W.H. Mechanical behaviour of laminated metal composites. *Int. Mater. Rev.* **1996**, *41*, 169–197. [CrossRef]
33. Shi, Z.F.; Guo, H.Z.; Zhang, J.W.; Yin, J.N. Microstructure−fracture toughness relationships and toughening mechanism of TC21 titanium alloy with lamellar microstructure. *Trans. Nonferrous Met. Soc. China* **2018**, *28*, 2440–2448. [CrossRef]
34. Ding, H.; Cui, X.P.; Gao, N.N.; Sun, Y.; Zhang, Y.Y.; Huang, L.J.; Geng, L. Fabrication of (TiB/Ti)-TiAl composites with a controlled laminated architecture and enhanced mechanical properties. *J. Mater. Sci. Technol.* **2021**, *62*, 221–233. [CrossRef]
35. Cui, X.; Fan, G.; Huang, L.; Gong, J.; Wu, H.; Zhang, T.; Geng, L.; Meng, S. Preparation of a novel layer-structured Ti_3Al matrix composite sheet by liquid–solid reaction between Al foils and TiB/Ti composite foils. *Mater. Des.* **2016**, *101*, 181–187. [CrossRef]
36. Qin, S.H.; Cui, X.P.; Tian, Z.; Geng, L.; Liu, B.X.; Zhang, J.E.; Chen, J.F. Synthesis and mechanical properties of innovative (TiB/Ti)-Ti_3Al micro-laminated composites. *J. Alloys Compd.* **2017**, *700*, 122–129. [CrossRef]
37. Zhu, H.; Sun, W.; Kong, F.; Wang, X.; Song, Z.; Chen, Y. Interfacial characteristics and mechanical properties of TiAl/Ti6Al4V laminate composite (LMC) fabricated by vacuum hot pressing. *Mater. Sci. Eng. A* **2019**, *742*, 704–711. [CrossRef]
38. Lyu, S.Y.; Sun, Y.B.; Ren, L.; Xiao, W.L.; Ma, C.L. Simultaneously achieving high tensile strength and fracture toughness of Ti/Ti-Al multilayered composites. *Intermetallics* **2017**, *90*, 16–22. [CrossRef]
39. Li, D.; Wang, B.; Luo, L.; Li, X.; Xu, Y.; Li, B.; Hawezy, D.; Wang, L.; Su, Y.; Guo, J.; et al. Effect of processing parameters on the microstructure and mechanical properties of TiAl/Ti_2AlNb laminated composites. *J. Mater. Sci. Technol.* **2022**, *109*, 228–244. [CrossRef]

Disclaimer/Publisher's Note: The statements, opinions and data contained in all publications are solely those of the individual author(s) and contributor(s) and not of MDPI and/or the editor(s). MDPI and/or the editor(s) disclaim responsibility for any injury to people or property resulting from any ideas, methods, instructions or products referred to in the content.